Proof-of-concept study of Coherent Point Drift registration for particle pairing in Particle Tracking Velocimetry

Bruno Mercier, Quriaky Gómez, Lionel Thomas, Benoit Tremblais, Laurent David

15th International Symposium on Particle Image Velocimetry – ISPIV 2023
June 19–21, 2023, San Diego, California, USA

Proof-of-concept study of Coherent Point Drift registration for particle pairing in Particle Tracking Velocimetry

B. Mercier[1*], Q. Gomez[1], L. Thomas[1], B. Tremblais[2], L. David[1]

[1] Institut P' CNRS, ISAE-ENSMA – UPR 3346, SP2MI, Poitiers, France
[2] Université de Poitiers, laboratoire XLIM, Axe ASALI/SRI, UMR7252 CNRS, Poitiers, France

[*] bertrand.mercier@univ-poitiers.fr

Abstract

The Coherent Point Drift (CPD) technique is applied for the first time to find pairs of particles between two subsequent sets of particles in the context of 3D Particle Tracking Velocimetry. Contrary to conventional method, CPD does not require any prior knowledge on the flow. The performances of this pairing method are quantitatively assessed on sets of particles generated from a synthetic turbulent flow. The method is found to provide consistent results for displacements up to two times the mean distance between particles, even when the number of ghost particles is equal to the number of true particles. The displacements obtained from the particle pairing are then successfully regularized to obtain velocity fields on a regular grid via an interpolation based on radial basis functions with a constraint on the divergence of the field.

1 Introduction

The development of methods for three-dimensional flow diagnostics over the last decade has certainly taken advantage of the emergence of new techniques for accurately identifying and determining particle positions from their projections on camera images Feng et al. (2007); Wieneke (2012); Schanz et al. (2016); Ben Salah et al. (2018); Mohr et al. (2019); Jahn et al. (2021); Acher et al. (2022). With the most advanced methods, particles can be localized in the images with an uncertainty in the order of 0.1 pixel for a density higher than 0.1 ppp (particle per pixel). These new capabilities may make Particle Tracking Velocimetry (PTV) more attractive than conventional Particle Image Velocimetry (PIV), even for two-dimensional cases that would benefit from the higher spatial resolution of PTV.

Once particles have been detected, the main challenge in PTV is to match the particles detected in one frame with the particles detected in a second subsequent frame. The pairing process is complex in itself, and is further complicated by the entry and exit of particles from the illuminated region in 2D measurements, and / or the detection of ghost particles in 3D measurements. A predictor that estimates the expected displacement of particles is commonly used to address this difficulty. The displacements can be estimated either from the local flow velocity determined with PIV techniques (Cowen et al. (1997)), or by extrapolation of previous particle positions along its trajectory (Schanz et al. (2016)). Other approaches to address the pairing problem which do not rely on any *a priori* knowledge are also under development (Zhang et al. (2015); Nie et al. (2021); Yang and Heitz (2021)). In general, the aim of these methods is to estimate the probability of a match between an arbitrary pair of particles in the two images. Likewise, we introduce in this contribution the coherent point drift (CPD) (Myronenko and Song (2010)) method which is used for the first time in the context of particle pairing for PTV. CPD belongs to the family of point set registration techniques which are used in computer vision to match two clouds of points that have undergone non-rigid deformations.

The following briefly describes the CPD method and provides an assessment of its limitations. In addition, a meshless regularization following principles described by Sperotto et al. (2022) with physical constrains is applied to the displacement fields obtained by CPD. The resultant velocity field is robust to noise and can be evaluated on a regular grid. Finally, the developed method is applied to a three-dimensional synthetic and realistic test case representing a turbulent mixing layer.

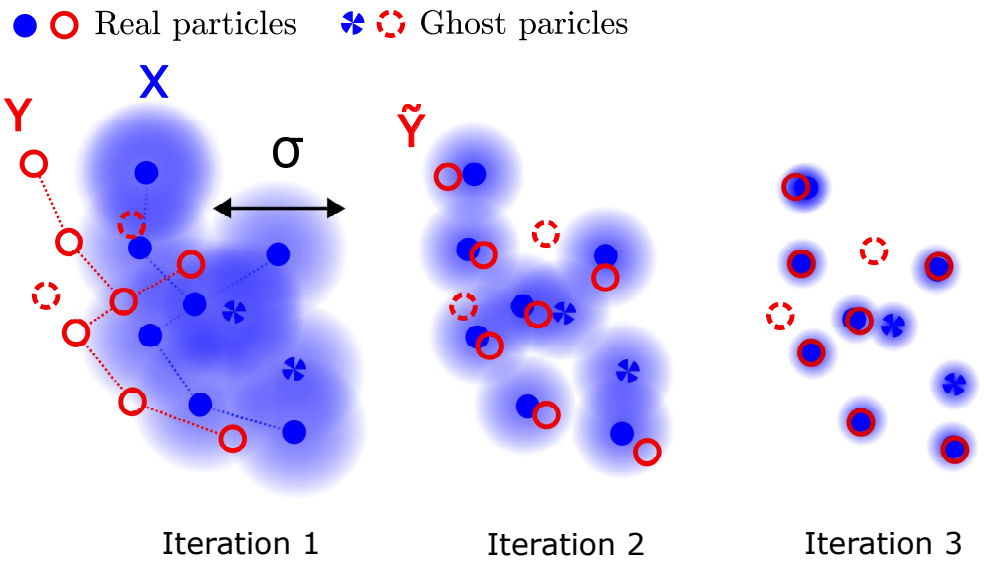

Figure 1: Schematic view of the iterative EM algorithm to register dataset $\mathbf{Y}$ to $\mathbf{X}$ with CPD. In this example the 7 pairs of particles are identified, and the four ghosts are discarded.

2 Coherent Point Drift

2.1 Principle of Coherent Point Drift

Coherent Point Drift (CPD) is a point-set registration algorithm which was first introduced by Myronenko et al. (2006), and that is used to align two sets of points in space.

In the context of double-frame velocimetry, the two sets of points are respectively the M particles detected in frame 1 (referred to as source points) and the N particles in frame 2 (referred to as target points), both being represented by their coordinates $\mathbf{Y} \in \mathbb{R}^{M\times D}$ and $\mathbf{X} \in \mathbb{R}^{N\times D}$, where $D = 2$ or 3 is the dimension of the problem. The result of the coherent point drift is a geometrical transformation $\mathcal{T}(\mathbf{Y},\theta)$ which maximizes the match between the transformed source $\tilde{\mathbf{Y}} = \mathbf{Y} + \mathcal{T}(\mathbf{Y},\theta)$ and the target $\mathbf{X}$, θ being the set of parameters that defines the transformation. Myronenko and Song (2010) derived three distinct algorithms for rigid, affine, and non-rigid deformations. The latter is the best suited for paring particles advected by a turbulent flow. The non-rigid transformation is modeled by a gaussian mixture model which centroids are initially aligned with the source points, and gaussian are weighted by the set of parameters θ that are computed by minimizing the negative-likelihood function $E(\theta,\sigma)$ which in its simplest form is given by Eq. (1)

$$E(\theta,\sigma) = -\sum_{n=1}^{N} \log \sum_{m=1}^{M} e^{-\frac{||X_n - Y_m - \mathcal{T}(Y_m,\theta)||^2}{2\sigma^2}}. \tag{1}$$

Myronenko and Song (2010) also add an additional term which accounts for noise and outliers. The problem is solved by an iterative Expectation–Maximization (EM) algorithm. Namely, a value for σ is guessed for the first iteration, and Equation (1) is minimized over θ under some constrains to enhance spatial coherence in the deformation. A value for σ is computed for the next iteration as an image of the distance between the coordinates of $\mathbf{X}$ and the updated coordinated $\tilde{\mathbf{Y}}$. The value of σ decreases after each iteration which allows to decouple unpaired particles from the minimization problem. After convergence, particles source that are found close to target particles with respect to the distance σ are likely to be paired, whereas particles that have no close neighbors are outliers. An heuristic description of this process is proposed in Fig. 1, nonetheless, the reader is invited to refer to Myronenko and Song (2010) for a comprehensive description of the method.

In the original method proposed by Myronenko et al. (2006), the initial value for σ is set arbitrarily to be similar to the spatial extent of the domain that contains the datasets. This arguably leads to slow convergence, so an initialization step has been developed to allow calculation of a first relevant value for σ. In this step, the first likelihood is estimated from the frozen turbulence assumption that states that local

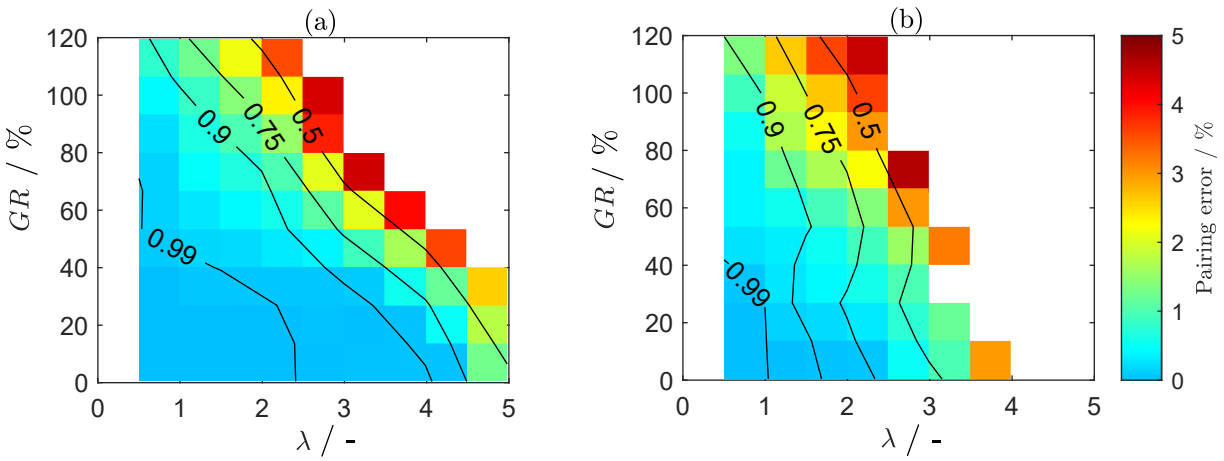

Figure 2: Map of the pairing error against the displacement ratio λ and the ghost to paired particles ratio *GR* for 5% (a) and 20% (b) turbulent intensity. The contours show the corresponding ratio of found pairs to total number of pairs. (Data are linearly interpolated from a coarser grid)

geometrical features that each particle depicts with its closest neighbors is hardly affected by the advection of the particles. These features are angles or distance ratios, and depend only on the local topology of the cloud of detected particles.

2.2 Performances of Coherent Point Drift

The robustness of the CPD for the pairing of particles is tested in the context of three-dimensional particle tracking velocimetry in a turbulent flow. The data sets consist of virtual particles. These particles could have been detected in a pair of images using standard methods, and therefore contain false detections. In the following, The number of paired particles is set to 2000, and an additional number of ghost particles is added in each frame of the data set at random position. The ghost ratio *GR*, defined as the number of ghosts divided by the number of paired particles, determines the number of ghosts. *GR* varies between 0 and 120 %. Paired particles are advected between the two frames in a synthetic velocity field implemented according to the method proposed by Martinez-Sanchis et al. (2021). The velocity field is representative of an isotropic and homogeneous turbulent flow with a mean velocity of $\overline{u}$=5 m/s, a convective velocity of 2.5 m/s, an integral length scale of 0.1 m and a Kolmogorov length scale of 1×10^{-5} m. Two levels of turbulence intensity $u'_{rms}/\overline{u}$ to assess the robustness of CPD with respect to the spatial decoherence of the pattern drawn by the particles, one is 5%, the second intensity is 20%. The average distance between neighbor particles $\overline{d}$ is kept equal to 0.4 mm and are advected in average by the distance d_{adv}. The displacement ratio $\lambda = d_{adv}/\overline{d}$ is varied between 0.5 and 5 by changing the time interval between the frames. For instance, the corresponding time interval for $\lambda = 1$ is 8×10^{-5} s, thus the corresponding frame rate is 12.5 kfps. Results are summarized in Fig. 2 which displays the pairing error against λ and *GR*, and the ratio of found pairs to total number of pairs. For both turbulence intensity, 90% of the pairs can be found with less than 1.5 % error up to a ghost ratio of 120 % for $\lambda \leq 1$. The pairing error, and the number of lost pairs, increase for higher λ, especially for the 20 % turbulence intensity. In case there are few ghost particles in the data set, say less than 20%, 75% of the pairs can still be found up to $\lambda = 4$ for 5 % turbulence intensity, and up to $\lambda = 2$ for 20 % with less than 1% of false pairing. For $GR = 60$ %, λ should remain under 3 for 5% of turbulence, and under 2 for 20%, yet with pairing errors remaining smaller than 2%.

3 Regularization

Displacement vectors obtained from particle pairing are inherently affected by the localization error of the particles and are sparsely distributed in space. These two concerns can be addressed by the addition of a regularization step to the data processing in order to both reduce the amplitude of the noise and interpolate the

data onto a regular grid. The chosen regularization strategy is based on the radial basis function formulation proposed by Sperotto et al. (2022).

3.1 Radial Basis Function formulation

The regularization proposed by Sperotto et al. (2022) consists in approximating the sparse displacement (*i.e.* velocity) data by a continuous function defined by a weighted sum of radial basis functions (RBF) $\varphi(\mathbf{X}, \mathbf{X_b^i}, \sigma_{reg})$, such that the displacement $\mathbf{U}(\mathbf{X})$ at the position of coordinates $\mathbf{X}$ is

$$\mathbf{U}(\mathbf{X}) = [u\ v\ w]^{\mathrm{t}}(\mathbf{X}) = \sum_{i=1}^{n_b} [\omega_u^i\ \omega_v^i\ \omega_w^i]^{\mathrm{t}}\ \varphi(\mathbf{X}, \mathbf{X_b^i}, \sigma_{reg}) \tag{2}$$

where σ_{reg} sets the size of the RBF, and $\mathbf{X_b} \in \mathbb{R}^{n_b \times D}$ are the coordinates of the n_b centroids of the RBF.

Here, the RBF are Gaussians of the form:

$$\varphi(\mathbf{X}, \mathbf{X_b^i}, \sigma_{reg}) = \exp\left(-\frac{\|\mathbf{X} - \mathbf{X_b^i}\|^2}{2\sigma_{reg}^2} \right). \tag{3}$$

The weighting coefficients ω_u, ω_v, and ω_w are determined by minimizing the norms

$$\begin{aligned} &||\Phi\omega_{\mathbf{u}} - \mathbf{v_s}||^2 \\ &||\Phi\omega_{\mathbf{v}} - \mathbf{v_s}||^2, \\ &||\Phi\omega_{\mathbf{w}} - \mathbf{w_s}||^2, \end{aligned} \tag{4}$$

evaluated for the n_s points of coordinates $\mathbf{X_s} \in \mathbb{R}^{n_s \times D}$ where the displacement $\mathbf{U_s} \in \mathbb{R}^{n_s \times D}$ were determined by CPD. The matrix $\Phi \in \mathbb{R}^{n_s \times n_b}$ contains the RBF $\varphi(\mathbf{X_s}, \mathbf{X_b^i}, \sigma_{reg})$. If the flow is incompressible, and the measurement domain is three-dimensional, a further constraint can be added in this formulation to ensure the divergence of the velocity field is zero as described in Sperotto et al. (2022). This however involves building and processing a matrix $\mathfrak{P} \in \mathbb{R}^{3n_s \times 3n_b}$ which can rapidly overwhelm the capabilities of the processing unit. For that reason, the measurement domain must be divided in subdomains that contains a reasonable number of displacement vectors.

3.2 Implementation with subdomains

Performing regularization on subdomains raises concerns at the boundaries between subdomains where continuity of velocity fields must be preserved. To solve this problem, a method derived from Ratz et al. (2022) is implemented. In practice, subdomains are overlapping with each other. In the overlap region, the velocity is a weighted average of the velocity computed from the two subdomains, where the weight is a function of the distance from the center of the sub-domain. Contrary to Ratz et al. (2022) who used circular domains, we use square ones which are more efficient to tessellate a volume. We also add a buffer layer outside the outer boundary of the subdomains, which is not considered by the weighting average, to account for the possible lack of consistency of the velocity field calculated there.

4 Example with double-frame synthetic data

A first assessment of the CPD pairing performances is carried out on a set of virtual particles advected by a synthetic flow. The flow which axial component is illustrated in Fig.3(a) over a surface at constant z. It features the characteristics of a sheared layer with a velocity varying linearly from 0 m/s to 5 m/s, with a turbulence intensity ratio of 10% and a Reynolds number of 10^4 based on the integral length scale of 10^{-2} m. The flow is seeded with 100,000 particles that are advected for 10×10^{-5} s (equivalent to a laser pulsing at 10 kHz) to generate two sets of particles coordinates corresponding to the results of a particle detection in two subsequent volumes of size $0.1 \times 0.1 \times 0.01\mathrm{m}^3$. Additionally, 50 % more randomly distributed particles are further added in each frame to simulate an imperfect detection and ghosts. In total, 150,000 particles are considered in the measurement volume. They are in average 0.4 mm away from its closest neighbor, and

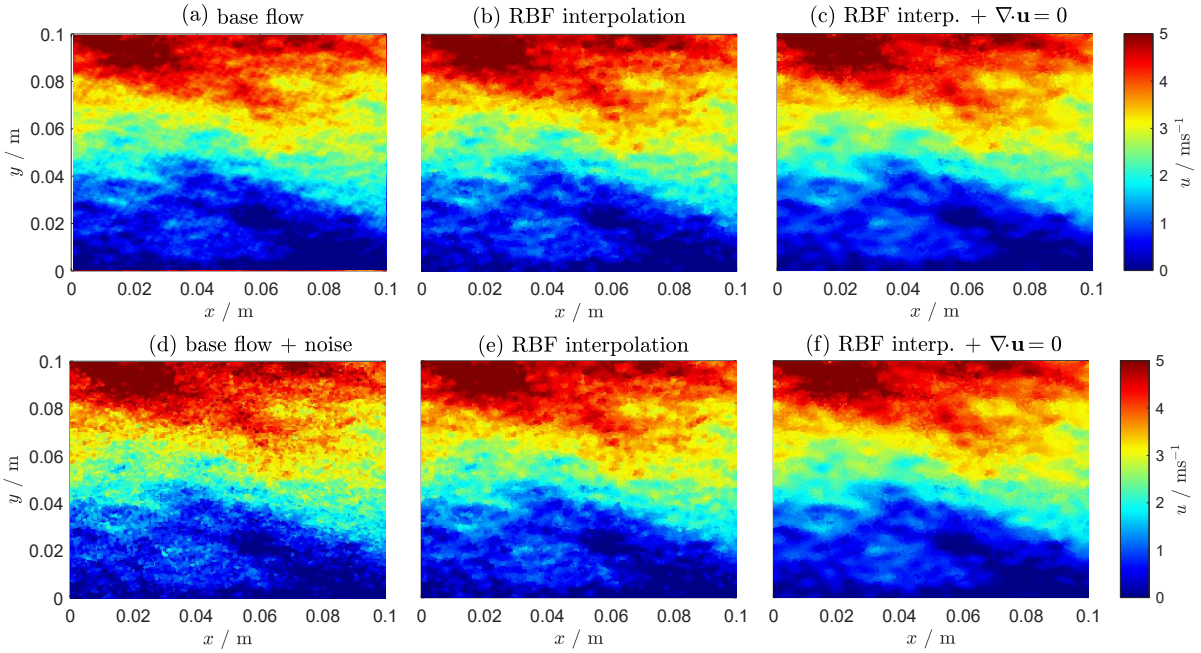

Figure 3: (b-c-e-f) Synthetic velocity fields reconstructed from the base flow clean of noise (a) and with noise (b).

their mean displacement is 0.18 mm between the two frames. The above described CPD and regularization are applied to these sets of particles corresponding to the base flow in Fig.3(a), and to the same base flow but with a random shift added to the positions of particles, resulting in the flow depicted in Fig.3(d). The standard deviation of this error is 4% of the maximum displacement. It corresponds to a 0.2 pixel detection error for a maximum displacement of 5 pixels in images. Figures 3(b) and (c) show the velocity field reconstructed from the radial basis functions (RBF) only, while a divergence-free constraint is applied in Figs 3(d) and (e). For these configurations, the RBF were supported by a regular grid with a spacing of 1 mm, thus approximately equal to twice the mean distance between particles. The value of σ_{reg} is set to 2.5 mm. Comparing noisy and clean cases leads to the first noticeable observation that the regularization is robust against the noise. The noise indeed tends to drop due to the averaging over the fairly large number of particles that lay within a distance of less than few σ_{reg} from the center of each RBF. Remarkably, despite this averaging effect, the small structures are well preserved by the regularization if the divergence is not constrained. This latter constrain indeed smoothes the reconstructed velocity fields, which may be beneficial to compute derived quantities such as the vorticity or the pressure field.

The duration of the 150,000 particle pairing with CPD together with the regularization is 8 minutes in total with a middle-end laptop (CPU I7-12850HX). The code is currently running on Matlab, thus better performances are expected after it is implemented in C++ and integrated in the in-house framework.

5 Conclusions

Particle tracking velocimetry has benefited greatly from the development of techniques to identify particles in images and to localize them in space. However, there has been no recent breakthrough in particle pairing techniques between images in the context of double-pulse velocimetry as there has been with shake-the-box for time-resolved data. This paper introduces the coherent point-drift particle pairing method with the aim of providing such a breakthrough. The method is found to be robust with respect to spurious and ghost particles for the displacements of the particles between two frames even for large displacements. A regularization of the measured displacements was performed and allowed to reconstruct a velocity field constrained to be divergence-free. Promising results are obtained for a realistic three-dimensional test case that includes small-scale turbulence and detection noise. This test provides a convincing proof of concept of the CPD method for PTV.

Future developments will aim to robustly handle the possible presence of masking objects in the measurement volume. The method will then be integrated into a time-resolved framework.

6 Acknowledgements

The authors would like to thank the ERDF of the Nouvelle Aquitaine Region for their financial support to the Grinfil project (Convention P-2020-BAFE-33) as well as the ANR through the France relance plan (Convention ANR-21-PRRD-0001-01) .

References

Acher G, Thomas L, Tremblais B, and David L (2022) A new camera model combining an analytical model and a discrete correction to overcome refractive index variation challenges. *Measurement Science and Technology* 33:125204

Ben Salah R, Alata O, Tremblais B, Thomas L, and David L (2018) Tomographic reconstruction of 3d objects using marked point process framework. *Journal of Mathematical Imaging and Vision* 60:1132–1149

Cowen EA, Monismith SG, Cowen EA, and Monismith SG (1997) A hybrid digital particle tracking velocimetry technique. *Experiments in Fluids* 22:199–211

Feng Y, Goree J, and Liu B (2007) Accurate particle position measurement from images. *Review of Scientific Instruments* 78:053704

Jahn T, Schanz D, and Schröder A (2021) Advanced iterative particle reconstruction for lagrangian particle tracking. *Experiments in Fluids* 62:179

Martinez-Sanchis D, Sternin A, Sternin D, Haidn O, and Tajmar M (2021) Analysis of periodic synthetic turbulence generation and development for direct numerical simulations applications. *Physics of Fluids* 33:125130

Mohr DP, Knapek CA, Huber P, and Zaehringer E (2019) Algorithms for particle detection in complex plasmas. *Journal of Imaging* 5

Myronenko A and Song X (2010) Point set registration: Coherent point drift. *IEEE Transactions on Pattern Analysis and Machine Intelligence* 32:2262–2275

Myronenko A, Song X, and Carreira-Perpiñán M (2006) Non-rigid point set registration: Coherent point drift. in B Schölkopf, J Platt, and T Hoffman, editors, *Advances in Neural Information Processing Systems*. volume 19. MIT Press

Nie M, Pan C, Wang J, and Cai C (2021) A hybrid 3d particle matching algorithm based on ant colony optimization. *Experiments in fluids* 62

Ratz M, Sachs S, König J, Mendez M, and Cierpka C (2022) Radial basis function regression of lagrangian three-dimensional particle tracking data. in *20th International Symposium on Application of Laser and Imaging Techniques to Fluid Mechanics*

Schanz D, Gesemann S, and Schröder A (2016) Shake-the-box: Lagrangian particle tracking at high particle image densities. *Experiments in Fluids* 57:70

Sperotto P, Pieraccini S, and Mendez MA (2022) A meshless method to compute pressure fields from image velocimetry. *Measurement Science and Technology* 33:094005

Wieneke B (2012) Iterative reconstruction of volumetric particle distribution. *Measurement Science and Technology* 24:024008

Yang Y and Heitz D (2021) Kernelized lagrangian particle tracking. *Experiments in Fluids* 62:252

Zhang Y, Wang Y, Yang B, and He W (2015) A particle tracking velocimetry algorithm based on the voronoi diagram. *Measurement Science and Technology* 26:075302